Fast, background-free, 3D super-resolution optical fluctuation imaging (SOFI)

T. Dertinger[a,1], R. Colyer[a], G. Iyer[a], S. Weiss[a,b,c,1], and J. Enderlein[d,1]

Departments of [a]Chemistry and Biochemistry and [b]Physiology, and [c]California NanoSystems Institute, University of California, Los Angeles, CA 90095; and [d]III. Institute for Physics, Georg-August-University, 37073 Göttingen, Germany

Edited by John W. Sedat, University of California, San Francisco, CA, and approved October 29, 2009 (received for review July 15, 2009)

Super-resolution optical microscopy is a rapidly evolving area of fluorescence microscopy with a tremendous potential for impacting many fields of science. Several super-resolution methods have been developed over the last decade, all capable of overcoming the fundamental diffraction limit of light. We present here an approach for obtaining subdiffraction limit optical resolution in all three dimensions. This method relies on higher-order statistical analysis of temporal fluctuations (caused by fluorescence blinking/intermittency) recorded in a sequence of images (movie). We demonstrate a 5-fold improvement in spatial resolution by using a conventional wide-field microscope. This resolution enhancement is achieved in iterative discrete steps, which in turn allows the evaluation of images at different resolution levels. Even at the lowest level of resolution enhancement, our method features significant background reduction and thus contrast enhancement and is demonstrated on quantum dot-labeled microtubules of fibroblast cells.

cumulants | fluorescence | quantum dots | superresolution microscopy | intermittency

Fluorescence microscopy permits 3D investigation of living cells, tissues, and even small organisms. However, features smaller than approximately half the emission wavelength (≈200–300 nm) cannot be resolved in conventional far-field microscopy because of the optical diffraction limit (1). Other techniques, such as electron microscopy (transmission electron microscopy, cryoEM) and scanning probe microscopy (scanning tunneling microscopy, atomic force microscopy), achieve molecular-level resolution, but are not suitable for imaging features within live cells. During the last decade, the optical diffraction limit has been overcome with the introduction of several new concepts, pioneered by stimulated emission depletion (STED) (2), ground-state depletion (3), structured illumination microscopy (SIM), (4, 5), and image interference microscopy (6). Stochastic techniques using photoswitchable probes have also been developed such as photo-activated localization microscopy (fPALM) (7), stochastic optical reconstruction microscopy (STORM) (8), PALM (9), and variants thereof (10, 11). The development of switchable fluorescent probes also triggered the emergence of new contrast enhancing techniques such as optical lock-in detection (OLID) (12). Even though OLID provides fast imaging with enhanced contrast, it lacks super-resolution capability. Conversely PALM and STORM achieve nanometer resolution, but with the tradeoff of slow acquisition speed (minutes to hours). STED has achieved video rate (13) but the method is quite demanding in terms of labeling procedures and choice of dyes and requires tedious alignment procedures. Recently, superresolution microscopy at 11 Hz has been demonstrated by using SIM, achieving a 2-fold increased lateral resolution (14). All super-resolution methods are capable of enhancing resolution in 3D, but often at the expense of major technical demands or modifications to the microscope (15–17).

Here, we report on a 3D super-resolution method that not only overcomes the diffraction limit, but also generates virtually background-free, contrast-enhanced images with a few seconds of acquisition time. Because it is based on the analysis of temporal fluorescence fluctuations of emitters (e.g., fluorescence intermittency), we call it super-resolution optical fluctuation imaging (SOFI). We demonstrate SOFI by using a conventional wide-field microscope equipped with a CCD camera, although in principle it can be applied to any kind of fluorescence imaging method (spinning disk, scanning confocal, total internal reflection, etc.). SOFI does not require controlled or synchronized photoactivation, but instead relies on the independent stochastic fluctuations of the emitters. Furthermore, SOFI works without the need for sophisticated electronics or acquisition schemes. It only involves taking a movie of the sample. However, three conditions must be met:

1. The fluorescent label has to exhibit at least two different emission states. For example, these states can be a fluorescent and a nonfluorescent one, but in principle any two or more states that are optically distinguishable will do.
2. Different emitters have to switch between states repeatedly and independently from each other in a stochastic way.
3. For this approach, the image should be acquired with pixels smaller than the diffraction limit. Resolution less than the pixel size will be the topic of a future publication.

These conditions being met, the pixel value of a SOFI image (of the order n) is obtained from the nth-order cumulant of the original pixel time series. The signal in a pixel using conventional imaging applications is given by the superposition of the fluorescence originating from different, nearby emitters. The nth-order cumulant (a quantity related to the nth-order correlation function) filters this signal based on its fluctuations in such a way that only highly correlated fluctuations are left over. In practice the remitting signal is limited to emitters within the pixel. The fluorescence signal contribution of these emitters to neighboring pixels will nonlinearly yield lower correlation values, leading to an increased resolution. The following section describes the underlying theory.

Theory

Given a sample composed of N single, independently fluctuating emitters, located at position $\mathbf{r}_k$ (Fig. 1*A*) and having a time-dependent molecular brightness $\varepsilon_k \cdot s_k(t)$, the resulting fluorescence source distribution is given by:

Author contributions: T.D., S.W., and J.E. designed research; T.D., R.C., and G.I. performed research; R.C. contributed new reagents/analytic tools; T.D. and R.C. analyzed data; and T.D. wrote the paper.

The authors declare no conflict of interest.

This article is a PNAS Direct Submission.

[1]To whom correspondence may be addressed. E-mail: t.dertinger@chem.ucla.edu, sweiss@chem.ucla.edu, or joerg.enderlein@physik3.gwdg.de.

This article contains supporting information online at www.pnas.org/cgi/content/full/0907866106/DCSupplemental.

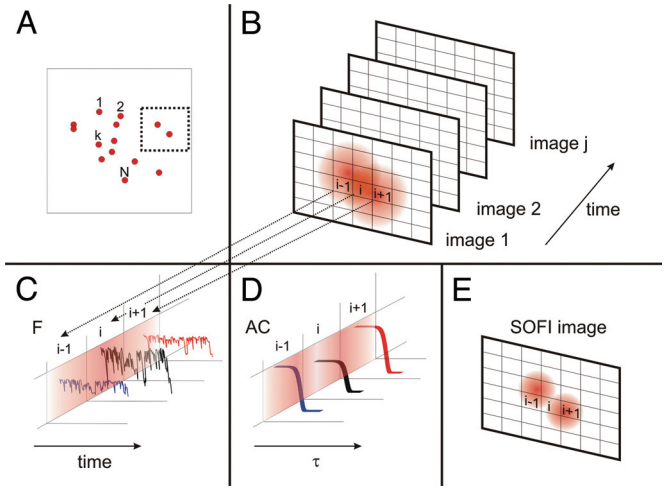

Fig. 1. Principle of SOFI. (*A*) Emitter distribution in the object plane. Each emitter exhibits fluorescence intermittency, which is uncorrelated with the others. (*B*) Magnified detail of the dotted box in *A*. The signal from the emitter fluorescence distribution is convolved with the systems PSF and recorded on a subdiffraction grid (e.g., pixels of the CCD-camera). Two neighboring emitters, for example, cannot be resolved because of the optical diffraction limit. The fluctuations are recorded in a movie. (*C*) Each pixel contains a time trace, which is composed of the sum of individual emitter signals, whose PSFs are reaching into the pixel. (*D*) The second-order correlation function is calculated from the fluctuations for each pixel. (*E*) The SOFI intensity value assigned for each pixel is given by the integral over the second-order correlation function. The second-order correlation function is proportional to the squared PSF, thus increasing the resolution of the imaging system by a factor of $\sqrt{2}$.

$$\sum_{k=1}^{N} \delta(\mathbf{r} - \mathbf{r}_k)\cdot\varepsilon_k\cdot s_k(t), \qquad [1]$$

where ε_k is the constant molecular brightness and $s_k(t)$ is a time-dependent fluctuation.

We assume that the positions of emitters do not change during the image acquisition; temporal changes are caused only by changes in the fluorescent states of individual emitters (e.g., blinking). For reason of simplicity we assume further that the point spread function (PSF) does not vary locally because of e.g., aberrations or polarization effects. However, such effects can be taken into account.

The fluorescence signal $F(\mathbf{r},t)$ at position $\mathbf{r}$ and time t is given by the convolution of the system's PSF $U(\mathbf{r})$ and the fluorescence source distribution (Eq. **1** and Fig. 1 *B* and *C*):

$$F(\mathbf{r}, t) = \sum_{k=1}^{N} U(\mathbf{r} - \mathbf{r}_k)\cdot\varepsilon_k\cdot s_k(t). \qquad [2]$$

Assuming that the sample is in stationary equilibrium during acquisition, the fluctuations can be expressed as zero-mean fluctuations:

$$\begin{aligned}\delta F(\mathbf{r}, t) &= F(\mathbf{r}, t) - \langle F(\mathbf{r}, t)\rangle_t \\ &= \sum_k U(\mathbf{r} - \mathbf{r}_k)\cdot\varepsilon_k\cdot[s_k(t) - \langle s_k(t)\rangle_t] \\ &= \sum_k U(\mathbf{r} - \mathbf{r}_k)\cdot\varepsilon_k\cdot\delta s_k(t), \qquad [3]\end{aligned}$$

where $\langle\ldots\rangle_t$ denotes time averaging. The second-order autocorrelation function $G_2(\mathbf{r},\tau)$ is then given by (see Fig. 1*D*):

$$\begin{aligned}G_2(\mathbf{r}, \tau) &= \langle\delta F(\mathbf{r}, t + \tau)\cdot\delta F(\mathbf{r}, t)\rangle_t \\ &= \sum_{j,k} U(\mathbf{r} - \mathbf{r}_j)U(\mathbf{r} - \mathbf{r}_k)\cdot\varepsilon_j\cdot\varepsilon_k\cdot\langle\delta s_l(t + \tau)\delta s_k(t)\rangle \\ &= \sum_k U^2(\mathbf{r} - \mathbf{r}_k)\cdot\varepsilon_k^2\cdot\langle\delta s_k(t + \tau)s_k(t)\rangle. \qquad [4]\end{aligned}$$

In Eq. **4** we assumed that the emission of different emitters is not correlated in time so that all cross-correlation terms $\langle\delta s_j(t + \tau)\delta s_k(t)\rangle$ with $j \neq k$ vanish. The second-order autocorrelation function thus appears as a simple sum of the squared PSF, weighted by each emitter's squared brightness and molecular correlation function $\langle\delta s_k(t + \tau)\delta s_k(t)\rangle$.

The value of $G_2(\mathbf{r},\tau)$ for a time lag τ defines a SOFI image, the only difference between each image being the weighting of the squared PSF with the molecular correlation function. Note that the intensities of a SOFI image do not report directly on the fluorescence signal, but rather its brightness and its degree of correlation. Additionally, the PSF is replaced by a distribution that is the square of the original PSF.

If the original PSF of the optical system can be approximated by a 3D Gaussian distribution, it follows from Eq. **4** that the width of the "new" PSF is reduced by a factor of $\sqrt{2}$ along all three dimensions, thus increasing the optical resolution of the second-order SOFI image:

$$U(\mathbf{r}) = \exp\left(-\frac{x^2 + y^2}{2\omega_0^2} - \frac{z^2}{2\omega_{z0}^2}\right) \qquad [5]$$

$$\Rightarrow U^2(\mathbf{r}) = \exp\left(-\frac{x^2 + y^2}{2\tilde{\omega}_0^2} - \frac{z^2}{2\tilde{\omega}_{0z}^2}\right)$$

with $\tilde{\omega}_{0z} = \omega_{0z}/\sqrt{2}$ and $\tilde{\omega}_0 = \omega_0/\sqrt{2}$.

Because the second-order correlation function involves the square of the PSF it is natural to look into higher-order correlation functions, generate higher powers of the PSF, and therefore further increase the resolution. The nth-order correlation function is given by:

$$\begin{aligned}&G_n(\mathbf{r}, \tau_1, \ldots, \tau_{n-1}) \\ &\quad = \langle\delta F(\mathbf{r}, t)\delta F(\mathbf{r}, t + \tau_1)\cdots\delta F(\mathbf{r}, t + \tau_{n-1})\rangle_t. \qquad [6]\end{aligned}$$

G_n can be easily computed in a straightforward manner, because the above formula states that the acquired signal fluctuations have to be multiplied for $n - 1$ time lags to obtain G_n. To generate SOFI images of higher orders, it is, however, necessary to transform the nth-order correlation functions into nth-order cumulant functions $C_n(\mathbf{r},\tau_1,\ldots\tau_{n-1})$. The reason is that all cross-terms caused by lower-order correlation contributions are eliminated in cumulants, so that the nth-order cumulant consists only of terms containing the nth power of the PSF. This can be understood by considering the following example. To compute the fourth-order correlation function, one ultimately needs to correlate four photons in one pixel. These photons could originate from different emitters or from the same emitter. The latter case would straightforwardly yield super resolution. However, it is also possible that two of the four photons are coming from one emitter and two are from a different emitter. These pairs, too, would contribute to the fourth-order correlation but only with a squared PSF for each emitter (cross-terms of lower orders) concealing the fourth-power PSF contribution, which arises from fluctuations from only a single emitter. Cumulants do not contain these cross-terms. Thus, only the use of cumulants

will ensure super resolution. This is expressed through the following equation:

$$C_n(\mathbf{r}, \tau_1, \ldots, \tau_{n-1}) = \sum_k U^n(\mathbf{r} - \mathbf{r}_k)\varepsilon_k^n w_k(\tau_1, \ldots, \tau_{n-1}), \quad [7]$$

where $w_k(\tau_1,\ldots,\tau_{n-1})$ is a correlation-based weighting function, depending on the specific fluctuation properties of each emitter. Note that the exact expression for $w_k(\tau_1,\ldots,\tau_{n-1})$ depends on the order of the cumulants. Because the nth-order cumulant generates an image with an effective PSF that is the nth power of the original PSF, the resolution is enhanced by a factor $\sqrt{n}$ for a Gaussian PSF. For instance, the fourth-order cumulant results in a SOFI image that has a 2-fold increased resolution, whereas the 16th-order cumulant will result in a 4-fold resolution enhancement. Although there is no fundamental limit for resolution enhancement, there are practical ones. Because the PSF is raised to the nth power, so is the molecular brightness ε from each emitter. Thus, an emitter that has a 2-fold larger molecular brightness will appear 2^n times brighter in the nth-order SOFI image. Additionally, the weighting function $w_k(\tau_1,\ldots,\tau_{n-1})$ can alter the apparent intensity in the SOFI image. An emitter that does not fluctuate over time will not yield any correlation [i.e., the weighting function $w_k(\tau_1,\ldots,\tau_{n-1}) = 0$ and thus the emitter will not appear in the SOFI image], whereas an emitter that blinks yields a nonzero value for the weighting function and will show up in the SOFI image. The exact value for the weighting function is determined by the specific blinking behavior of the emitters. The product of the nth power of the molecular brightness and the weighting function of an individual emitter therefore determines its contribution to the SOFI image, which can lead to the masking of dim emitters that are in close proximity to bright emitters (see *SI Text* and Figs. S1 and S2). In other words, the resulting higher-order SOFI images have a very large dynamic intensity range. This effect reduces the apparent information content of the final SOFI image and is pronounced for orders > 2.

Although there is no fundamental difficulty in computing higher-order cumulants, it is worth noticing, that the nth-order cumulant is an $(n - 1)$-dimensional function of the τ_i. Therefore, the computation time and memory requirements are growing as n^2, which may be rapidly become a limiting factor for the generation of higher-order SOFI images. In practice, it is most efficient to compute SOFI images by setting all time lags to zero:

$$C_n(\mathbf{r}, 0) \equiv C_n(\mathbf{r}, \tau_1 = 0, \ldots, \tau_{n-1} = 0) = \sum_k U^2(\mathbf{r} - \mathbf{r}_k)\varepsilon_k^n w_k(0). \quad [8]$$

In this case the cumulant formulas can be expressed in a simplified form (e.g., the second-order cumulant becomes simply the variance of the signal), which is algorithmically easy to realize:

$$C_2(\mathbf{r}, 0) = \langle F^2(\mathbf{r}, 0)\rangle - \langle F(\mathbf{r}, 0)\rangle. \quad [9]$$

This simplification, of course, does not eliminate shot noise of the signal and is most likely not applicable, when the signal-to-noise ratio is low, as, for example, when measuring with organic dyes. In this case cumulants should be calculated in a shot-noise free manner as discussed in *SI Text* and Figs. S1 and S3.

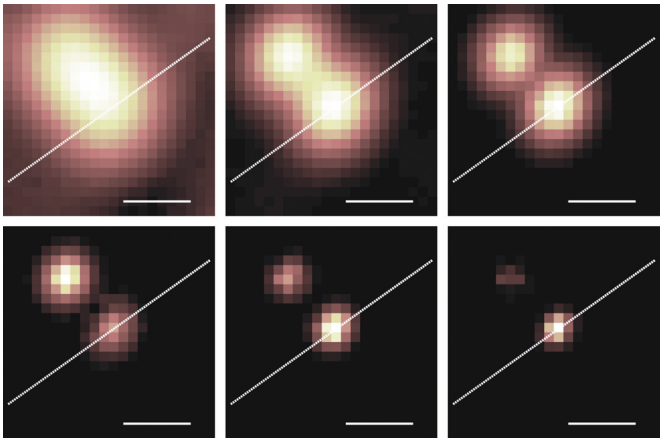

Fig. 2. Higher-order SOFI images. Selected SOFI images acquired from a movie taken with QDs deposited on a coverslip are shown. From upper left to lower right: Original image (mean intensity of all movie frames) and 2nd, 4th, 9th, 16th, and 25th orders of SOFI. The two different QDs are resolved at higher-order SOFI images. Note that the relative intensities of the two QDs vary depending on the specific blinking characteristics of each QD, which is addressed at different cumulant orders. The dotted cross-section lines are used in Fig. 3. (Scale bars: 250 nm.)

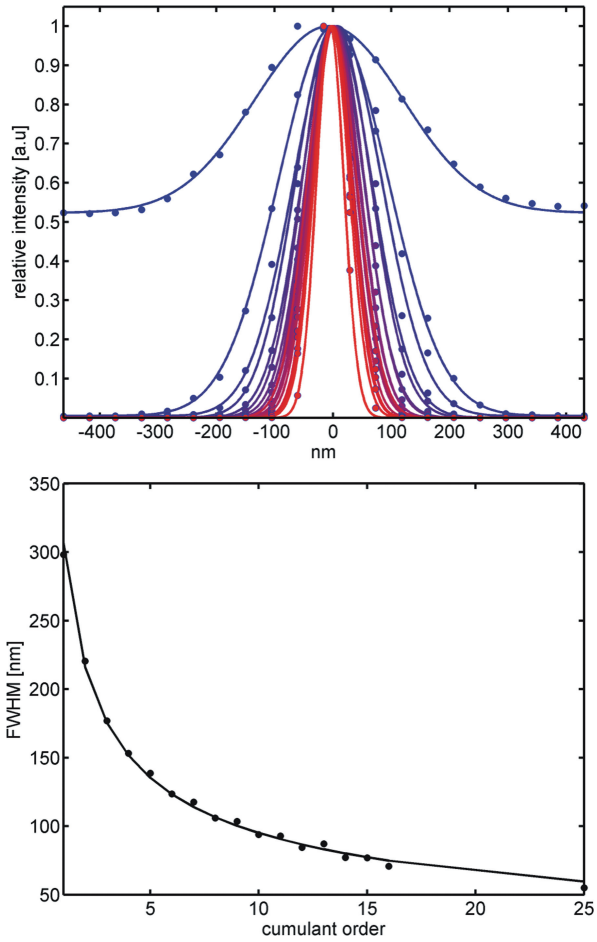

Fig. 3. Resolution enhancement of SOFI. (*Upper*) 1D Gaussian fits of the cross-sections displayed in Fig. 2. Plotted are the original intensity and the normalized cumulants orders 2–25. The cumulant order is increasing from blue to red. Lines show Gaussian fits. Dots indicate data. The original image intensities are offset because of background present in the image, whereas there is no background in the SOFI images and thus no offset. (*Lower*) Fitted FWHM (circles) as a function of cumulant order The line is a fit according to: FWHM $= \omega_{50} \cdot n^a$.

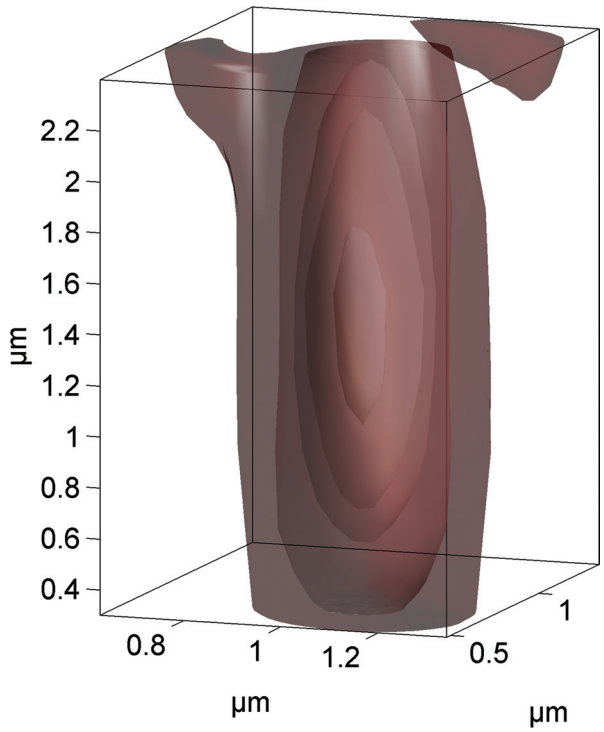

Fig. 4. 3D SOFI. Rendered 3D PSF composed of 2D sections taken along the *z* axis (300-nm steps). Surfaces were smoothed with a Gaussian smoothing algorithm. The isosurfaces for $I_{max} \cdot e^{-2}$ are shown. Starting from the outermost isosurface, the original PSF is shown followed by orders 2nd, 3rd, 4th, and 16th. PSF aberrations are noticeable at the top of the original PSF image.

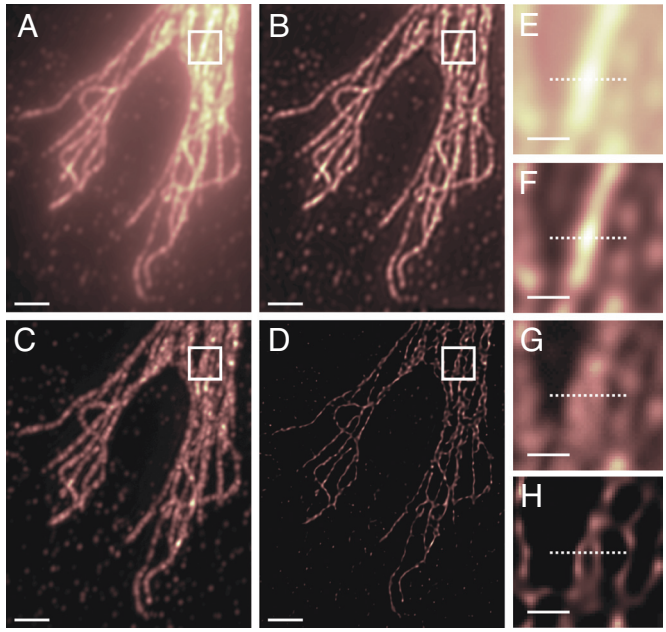

Fig. 5. SOFI images of cells. Wide-field image of QD625 labeled 3T3 cells. (*A*) Original image generated by time averaging all frames of the acquired movie (3,000 frames, 100 ms per frame). (*B*) The image in *A* deconvolved. (*C*) Second-order SOFI image. (*D*) The image in *C* deconvolved. (*E–H*) Magnified views of the boxed regions in *A–D*. (Scale bars: *A–D*, 2 μm; *E–H*, 500 nm.)

Results

We first demonstrate the concept of SOFI by using quantum dots (QDs) deposited on a coverslip. Because the QDs fluorescence on/off distributions obey a power law (18), they blink at all time scales, which allows the use of arbitrary camera frame rates. Data were recorded in series of 2,000 frames (100 ms per frame).

Because resolution is defined by the ability to differentiate between two close-by point sources, we first demonstrate resolution enhancement with a pair of QDs that are separated by a distance shorter than the diffraction limit. Fig. 2 shows the 2nd-, 4th-, 9th-, 16th-, and 25th-order cumulant SOFI images of two close-by QDs. It is clear from Fig. 2 that as the cumulant order is increased the PSF shrinks and the two QDs are better resolved. The dotted line in Fig. 2 denotes the cross-section through the PSF of a single QD. This intensity cross-section (Fig. 2, dotted line) was fitted with a 1D Gaussian model for all calculated cumulants orders. Fig. 3 *Upper* shows the profiles (dots) and the fits (lines). Note that the PSF in the original (intensity) image comprises an offset caused by constant, uncorrelated background signal, which disappears in the SOFI images. Comparing the signal-to-background (S/B) ratios of the original image with the second-order SOFI image, we observe a striking 130-fold improvement ($S/B_{original} = 1.9$; $S/B_{second\text{-}order} = 250$). Fig. 3 *Lower* shows the FWHM values of the Gaussian fits plotted versus the cumulant order. This curve was fitted with a power law: $FWHM(n) = \omega_{50} \cdot n^a$, n being the cumulants order and ω_{50} being the FWHM value of the raw image. The fit yielded $\omega_{50} = 289 \pm 2$ nm and $a = 0.51 \pm 0.01$, in agreement with the expected square-root scaling of the resolution enhancement with the cumulant order. The 25th-order yielded an image with a FWHM $= 55 \pm 3$ nm, corresponding to a 5-fold resolution enhancement in 2D. It is evident from Eq. **4** that the resolution enhancement takes place along all three dimensions. To prove this, we performed a 3D scan through a single QD. Movies were recorded for different image planes (300-nm spacing, 4,000 frames, 75 ms per frame), and SOFI images were generated for each plane. The smoothed e^{-2} iso-surfaces of these sections were rendered as a 3D image. The result is shown in Fig. 4, demonstrating that the SOFI's PSFs are shrinking along all three axes at higher orders. This was confirmed by 2D Gauss-fits along *x-z* cross-sections yielding the expected square-root law. The original image, however, was excluded from the fitting because of its non-Gaussian profile, rendering Gauss-fits inappropriate.

In a second experiment, the α-tubulin network of a 3T3 fibroblast cell was immuno-stained with QDs to evaluate the imaging capabilities of SOFI. Fig. 5 *A* and *C* shows the results for the original and the second-order SOFI images, respectively. In addition to the increase in resolution, a striking enhancement in S/B is apparent, because of the elimination of the hazy background present in the processed image, because the SOFI algorithm intrinsically removes uncorrelated background.

The background removal in SOFI images proves especially useful for an optional, subsequent image deconvolution. Because deconvolution algorithms tend to operate better if no background is present, we compared the performance of a commercially available deconvolution program (Huygens Professional) on the original intensity image and the corresponding second-order SOFI image. The results are shown in Fig. 5 *B* and *D*, respectively. As can be seen, the software performs well on the original wide-field image, and the quality of the deconvolved image is comparable with the second-order SOFI image. However, the second-order SOFI image can be deconvolved noticeably better, as demonstrated in Fig. 6, where intensity profiles of a cross-section from Fig. 5 *E–H* (box in Fig. 5 *A–D*) are compared. SOFI images of orders $n > 2$, did not lead to satisfying images because of extreme brightness differences within the image (Fig. S4).

Discussion

We have introduced a super-resolution technique and demonstrated that by using higher-order statistics the optical resolution

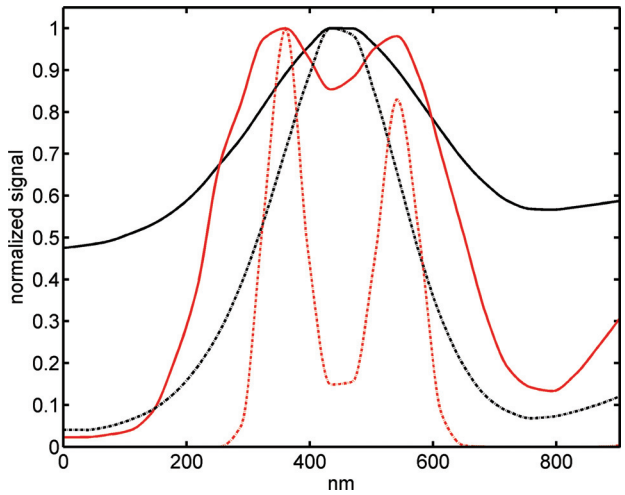

Fig. 6. Comparison of resolution enhancement of SOFI. Intensity profiles extracted from the dotted lines in Fig. 5 *E–H* are shown . Black solid line indicates original image. Red solid line indicatea second-order SOFI image. Dotted lines correspond to cross-sections taken from the deconvolved images. The second-order SOFI image clearly exhibits gain in resolution.

of a conventional microscope can be increased far beyond the diffraction limit ($\sqrt{n}$ times the FWHM of the PSF, where n is the statistical order) while simultaneously enhancing the image contrast. We argue that no other super-resolution microscopy technique can compete with the simplicity of the SOFI approach and its undemanding requirements with regard to fluorescent labels, optics, and other hardware. The experimental procedure essentially amounts to taking a movie of a fluctuating signal. Other correlation-based imaging methods such as image correlation spectroscopy (ICS) and related methods such as Raster ICS and spatiotemporal (STICS) (19, 20, 23), diffusion imaging (21), OLID, or fluorescence cumulant analysis (22) do not exploit the super-resolution imaging potential of higher-order statistics. Comparing SOFI specifically with STICS reveals a striking analogy in formulas, because both methods use image series and temporal correlations. However, in STICS spatial correlation images are calculated from each image (or parts thereof) combined with a temporal correlation on these spatial correlation images. The behavior of this spatiotemporal correlation image series allows the quantification and separation of molecular transport properties, although no super-resolution imaging. Lidke et al. (24) have developed a super-resolution imaging method that is based on independent component analysis and blinking statistics of QDs. They demonstrated that this method is capable to resolve QDs that are closely spaced below the diffraction limit. As pointed out by Lidke et al. underestimating or overestimating the number of QDs can affect the accuracy in determination of the loci of the (incorrect number of) emitters. In SOFI no such a priori knowledge is necessary.

Also dynamic speckle illumination microscopy (DSI) (25–27) is based on the evaluation of fluctuations in the observed signal, but ones that are induced by the excitation and subsequently evaluated in an analogous way to SOFI. Even though this approach yields sectioning along the optical axis, the fact that the fluctuations are not stemming from independent microscopic (i.e., subdiffraction sized) emitters but from diffraction limited speckles imposes a fundamental limit on DSI resolution, because it is diffraction limited. The similarities between SOFI and the above-mentioned methods have their origin solely in the common mathematical concept of correlation functions. However, a detailed analysis of these approaches reveals dramatic differences in capabilities and resulting effects.

We verified that the SOFI concept leads to an increase in optical resolution along all three directions. Furthermore we demonstrated that SOFI is suitable for biological imaging applications as shown on fluorescently labeled, fixed 3T3 fibroblasts, achieving background-free, contrast-enhanced, super-resolution images. An additional benefit of the SOFI images is that deconvolution algorithms tend to perform better on these background-free images.

The main limitation of SOFI is the brightness scaling of the images; the higher the order, the larger initial differences in brightness will grow. This results in very large dynamic range images and can lead to masking effects of dim emitters in proximity to bright emitters. SOFI can be regarded as a single-molecule technique, because it relies on the detection of fluctuations from single emitters. Even though SOFI theoretically eliminates any kind of noise (noise is per definition not correlated over time), it is sensitive to the signal-to-noise ratio because acquisition times are limited (e.g., caused by photobleaching). Limited measurement times lead to a "correlation" noise in SOFI, which is not any different from other correlation-based methods such as fluorescence correlation spectroscopy (FCS). There are several publications characterizing noise in FCS measurements (as, for example, refs. 28 and 29). To reduce noise in a SOFI image, measurement times have to be extended or the signal-to-noise ratio has to be improved until the desired image quality is achieved.

SOFI has the potential to perform super-resolution imaging, at high frame rates. The acquisition speed in this work was limited mainly by the blinking behavior of QDs. Because of their power-law fluorescence on/off distribution (18, 30–32), some QDs exhibit strong blinking, whereas others might remain in the on state for a few seconds of movie acquisition, leading to very different brightness values in the SOFI images. By choosing probes displaying a uniform blinking rate, one should be able to drastically shorten the acquisition times. Also, a more uniform blinking could help to resolve the brightness scaling problem of SOFI (because SOFI brightness depends on the molecular brightness and the molecular blinking behavior). In terms of flexibility, SOFI is not limited to work with high numerical aperture microscope objectives and thus could be used in imaging applications, where its main advantage could be background reduction. Last, SOFI is not limited to blinking between fluorescent on and off states. Any (even nonfluorescent) fluctuating objects, such as rotating dipoles, or blinking of celestial objects, such as binary stars, could be imaged and superresolved by SOFI.

Methods

All experiments were carried out using QD625 secondary antibodies (Invitrogen) QD. 3T3 cells were fixed and labeled by using a standard immunostaining protocol (for details refer to *SI Text*).

Microscope Setup and Data Analysis. Movies were taken on an inverted wide-field microscope (Olympus IX71, objective: UPlanApo 60×, 1.45, Oil). A 470-nm LED array device was used as a light source (Lumencor Aura Light Engine) and a CCD camera (Andor iXon + 885) was used to record the signal. Filter set was dichroic [505 DCXR, Chroma Technology; emission (D620/40, Chroma Technology]. Magnification was adjusted to obtain 35 nm per pixel. To generate and evaluate SOFI images, movies were analyzed by using a custom-written Matlab (Mathworks) code. The shortest accessible time lag is the frame integration time (time between two subsequent frames). We computed all SOFI images for the zero time lag only C_n (r,0,0,…0). In this case a computationally less expensive expression for the cumulants formula can be used (see *SI Text*). Cumulants of orders > 2 can turn negative depending on the underlying fluctuation pattern. SOFI images are therefore displayed as absolute values.

ACKNOWLEDGMENTS. We thank Xavier Michalet for extensive proofreading of the manuscript; Xiaoqun Zhang (University of California, Los Angeles) for advice in deconvolution; Prof. Vidvuds Ozolins (University of California, Los Angeles) for useful discussions; and Jeff M. Reece (Recent Technologies) and José Viña (Scientific Volume Imaging) for help with deconvolution. This work was supported by National Institutes of Health Grants 5R01EB000312 and 1R01GM086197. T.D. is supported by German Science Foundation Fellowship DE 1591/1-1. J.E. is supported by Human Frontier Science Program Grant RGP46/2006 and German Federal Ministry of Education and Research Grant FKZ 13N9236.

1. Abbe E (1873) Conributions to the theory of the microscope and the microscopic perception (translated from German). *Arch Mikr Anat* 9:413–468.
2. Hell SW, Wichmann J (1994) Breaking the diffraction resolution limit by stimulated emission: Stimulated-emission-depletion fluorescence microscopy. *Opt Lett* 19:780–782.
3. Hell SW, Kroug M (1995) Ground-state-depletion fluorescence microscopy: A concept for breaking the diffraction resolution limit. *Appl Phys B Lasers Optics* 60:495–497.
4. Gustafsson MGL (2000) Surpassing the lateral resolution limit by a factor of two using structured illumination microscopy. *J Microsc* 198:82–87.
5. Heintzmann R, Jovin TM, Cremer C (2002) Saturated patterned excitation microscopy: A concept for optical resolution improvement. *J Opt Soc Am A* 19:1599–1609.
6. Gustafsson MGL, Agard DA, Sedat JW (1999) (IM)-M-5: 3D wide-field light microscopy with better than 100-nm axial resolution. *J Microsc Oxford* 195:10–16.
7. Hess ST, Girirajan TPK, Mason MD (2006) Ultra-high-resolution imaging by fluorescence photoactivation localization microscopy. *Biophys J* 91:4258–4272.
8. Rust MJ, Bates M, Zhuang XW (2006) Subdiffraction-limit imaging by stochastic optical reconstruction microscopy (STORM). *Nat Methods* 3:793–795.
9. Betzig E, et al. (2006) Imaging intracellular fluorescent proteins at nanometer resolution. *Science* 313:1642–1645.
10. Folling J, et al. (2008) Fluorescence nanoscopy by ground-state depletion and single-molecule return. *Nat Methods* 5:943–945.
11. Heilemann M, et al. (2008) Subdiffraction-resolution fluorescence imaging with conventional fluorescent probes. *Angew Chem Int* 47:6172–6176.
12. Marriott G, et al. (2008) Optical lock-in detection imaging microscopy for contrast-enhanced imaging in living cells. *Proc Natl Acad Sci USA* 105:17789–17794.
13. Westphal V, et al. (2008) Video-rate far-field optical nanoscopy dissects synaptic vesicle movement. *Science* 320:246–249.
14. Kner P, et al. (2009) Super-resolution video microscopy of live cells by structured illumination. *Nat Methods* 6:339–342.
15. Shtengel G, et al. (2009) Interferometric fluorescent super-resolution microscopy resolves 3D cellular ultrastructure. *Proc Natl Acad Sci USA* 106:3125–3130.
16. Juette MF, et al. (2008) Three-dimensional sub-100-nm resolution fluorescence microscopy of thick samples. *Nat Methods* 5:527–529.
17. Huang B, Jones SA, Brandenburg B, Zhuang XW (2008) Whole-cell 3D STORM reveals interactions between cellular structures with nanometer-scale resolution. *Nat Methods* 5:1047–1052.
18. Kuno M, Fromm DP, Hamann HF, Gallagher A, Nesbitt DJ (2001) On/off fluorescence intermittency of single semiconductor quantum dots. *J Chem Phys* 115:1028–1040.
19. Petersen NO, Hoddelius PL, Wiseman PW, Seger O, Magnusson KE (1993) Quantification of membrane-receptor distributions by image correlation spectrscopy: Concept and application. *Biophys J* 65:1135–1146.
20. Brown, et al. (2008) Raster image correlation spectroscopy (RICS) for measuring fast protein dynamics and concentrations with a commercial laser scanning confocal microscope. *J Microsc* 229:78–91.
21. Roth CM, Heinlein PI, Heilemann M, Herten D-P (2007) Imaging diffusion in living cells using time-correlated single-photon counting. *Anal Chem* 79:7340–7345.
22. Müller JD (2004) Cumulant analysis in fluorescence fluctuation spectroscopy. *Biophys J* 86:3981–3992.
23. Hebert B, Costantino S, Wiseman PW (2005) Spatiotemporal image correlation spectroscopy (STICS) theory, verification, and application to protein velocity mapping in living CHO cells. *Biophys J* 88:3601–3614.
24. Lidke KA, Rieger B, Jovin TM, Heintzmann R (2005) Superresolution by localization of quantum dots using blinking statistics. *Optics Express* 13:7052–7062.
25. Ventalon C, Heintzmann R, Mertz J (2007) Dynamic speckle illumination microscopy with wavelet prefiltering. *Optics Lett* 32:1417–1419.
26. Ventalon C, Mertz J (2006) Dynamic speckle illumination microscopy with translated versus randomized speckle patterns. *Optics Express* 14:7198–7209.
27. Ventalon C, Mertz J (2005) Quasi-confocal fluorescence sectioning with dynamic speckle illumination. *Optics Lett* 30:3350–3352.
28. Qian H (1990) On the statistics of fluorescence correlation spectroscopy. *Biophys Chem* 38:49–57.
29. Koppel DE (1974) Statistical accuracy in fluorescence correlation spectroscopy. *Phys Rev A* 10:1938–1945.
30. Kuno M, Fromm DP, Hamann HF, Gallagher A, Nesbitt DJ (2000) Nonexponential ''blinking'' kinetics of single CdSe quantum dots: A universal power law behavior. *J Chem Phys* 112:3117–3120.
31. Chung I, Bawendi MG (2004) Relationship between single quantum-dot intermittency and fluorescence intensity decays from collections of dots. *Phys Rev B* 70:165304.
32. Frantsuzov P, Kuno M, Janko B, Marcus RA (2008) Universal emission intermittency in quantum dots, nanorods, and nanowires. *Nat Phys* 4:519–522.

Supporting Information

Dertinger et al. 10.1073/pnas.0907866106

SI Text

Preparing Samples. ***Preparing slides with spin-coated QDs.*** QD625 secondary antibodies (Invitrogen) were spin-coated on a coverslide. ***Preparing 3T3 cells.*** NIH 3T3 (ATCC) cells were grown up to a confluence level of ≈80% in DMEM (ATCC catalog no. 30-2002) plus 10% FCS (10082-147; Invitrogen) and 100 units of penicillin-streptomycin (Pen-Strep, 15140122; Invitrogen). For fixation the following procedure has been applied. Cells were incubated at room temperature for 15 min with CB buffer [10 mM Mes (pH 6.2), 140 mM NaCl, 2.5 mM EGTA, 5 mM $MgCl_2$], 11% sucrose, 3.7% paraformaldehyde, 0.5% glutaraldehyde, and 0.25% Triton as a fixative. Quenching was done with 0.5 mg/mL sodium borohydride in CB for 8 min. Cells were washed once with PBS and blocked in 2% BSA+PBS for 1 h at room temperature. Microtubules were stained by using 1:500 dilution of DM1A anti-α-tubulin monoclonal antibody (Sigma) in 2% BSA+PBS. Cells were then washed three times with PBS and incubated for 1 h at room temperature with a 1:400 dilution of QDs QD625-labeled goat $F(ab)_2$, anti-mouse IgG antibodies (H+L) (Invitrogen) in 6% BSA + PBS. Cells were washed three times with PBS. All steps were performed in a humidity chamber. Specimens were dehydrated by floating the coverslips sequentially for 5 s in 30%, 70%, 90%, and 100% ethanol. Subsequently, they were gently spin-coated (≈500 rpm; Specialty Coating Systems model P-6000 spin coater) with 1 mg/mL PVA. A movie (3,000 frames, 100 ms per frame) was acquired and subsequently analyzed with the SOFI algorithm

Ways to Calculate SOFI Images. SOFI is based on the calculation of the nth-order cumulant. The nth-order cumulant can be derived from the nth-order correlation function. Because there are many ways to calculate a SOFI image, we will discuss the different possibilities. This includes the calculation of shot noise-free SOFI images. Also the possibility to achieve SOFI images that contain less noise, from an existing dataset will be explained. Let us first start with the conversion of nth-order-correlation functions into cumulants.

On the Calculation of Cumulants. The nth-order cumulant C_n can be derived from the correlation functions G (shown only up to the fourth order). For the recursive formula see Mendel (1):

$$\begin{aligned} C_2(\mathbf{r}, \tau_1) &= G_2(\mathbf{r}, \tau_1) \\ C_3(\mathbf{r}, \tau_1, \tau_2) &= G_3(\mathbf{r}, \tau_1, \tau_2) \\ C_4(\mathbf{r}, \tau_1, \tau_2, \tau_3) &= G_4(\mathbf{r}, \tau_1, \tau_2, \tau_3) - G_2(\mathbf{r}, \tau_1)\cdot G_2(\mathbf{r}, \tau_3) - G_2(\mathbf{r}, \tau_1 + \tau_2)\cdot G_2(\mathbf{r}, \tau_2 + \tau_3) - G_2(\mathbf{r}, \tau_1 + \tau_2 + \tau_3)\cdot G_2(\mathbf{r}, \tau_2). \end{aligned} \quad \text{[S1]}$$

In the limit of very fast temporal sampling and short time lags with respect to blinking rates, one can approximate the above equation by a computationally less expensive formula. The formula to recursively derive these (approximated) cumulants C_i^{approx} from correlation functions is given by (2):

$$\begin{aligned} C_2^{approx}(\mathbf{r}, \tau_1) &= G_2(\mathbf{r}, \tau_1) \\ C_3^{approx}(\mathbf{r}, \tau_1, \tau_2) &= G_3(\mathbf{r}, \tau_1, \tau_2) \\ C_4^{approx}(\mathbf{r}, \tau_1, \tau_2, \tau_3) &= G_4(\mathbf{r}, \tau_1, \tau_2, \tau_3) \\ &\quad - 3\cdot(G_2(\mathbf{r}, \tau_1))^2 \\ &\vdots \\ C_n^{approx}(\mathbf{r}, \tau_1, \ldots, \tau_{n-1}) &= G_n(\mathbf{r}, \tau_1, \ldots, \tau_n) \\ &\quad - \sum_{i=1}^{n-1} \binom{n-1}{i} C_{n-i}^{approx}(\mathbf{r}, \tau_1, \ldots, \tau_{n-1-i}) G_i(\mathbf{r}, \tau_1, \ldots, \tau_{i-1}). \end{aligned} \quad \text{[S2]}$$

As can be seen from Eqs. **S1** and **S2**, the exact and approximated cumulants are identical for $\tau_i = 0$. We also did simulations to point out the differences (see *Simulation Results*).

Noise Reduction in SOFI Images. If acquisition times are short, there is the possibility to reduce noise in the SOFI image. Instead of calculating SOFI images for only the zero time lag, one can calculate SOFI images for many time lags and afterward sum all SOFI images. This time lag-integrated SOFI image contains less noise. In the following equation we used the expression for the nth-order cumulant $C_n(\mathbf{r},\tau_1,\ldots,\tau_{n-1})$ as given in e.g., Eq. **S1**.

$$I_n(\mathbf{r}) = \int_{t_1^1}^{t_1^2} \cdots \int_{t_{n-1}^2}^{t_{n-1}^2} C_n(\mathbf{r}, \tau_1, \ldots, \tau_{n-1}) d\tau_1 \ldots d\tau_{n-1} \propto U^n(\mathbf{r}), \quad \text{[S3]}$$

where the integration is carried out over as many time lags as needed. Obviously, values at long time lags tend to zero and eventually contribute little to the final integrated image.

SOFI Cross-Cumulant Approach. A more general approach to SOFI is to calculate the spatiotemporal cross-cumulant XC_n between different positions $\mathbf{r}_i$. The second-order cross-cumulant XC_2, for example, is given by [as can be easily derived an analogous approach as for the second-order autocorrelation (Eq. **5**)]:

$$XC_2(\mathbf{r}_1,\ \mathbf{r}_2,\ \tau) = \sum_k \langle \delta f_k(t+\tau)\cdot\delta f_k(t)\rangle_t U(\mathbf{r}_1-\mathbf{r}_k)U(\mathbf{r}_2-\mathbf{r}_k). \quad \textbf{[S4]}$$

Assuming a 3D Gaussian PSF (or a 2D Gaussian in the image plane), this expression can be simplified further by using

$$(\mathbf{r}_1-\mathbf{r})^2+(\mathbf{r}_2-\mathbf{r})^2 = 2\left(\left(\frac{\mathbf{r}_1+\mathbf{r}_2}{2}-\mathbf{r}\right)+\left(\frac{\mathbf{r}_1-\mathbf{r}_2}{2}\right)^2\right), \quad \textbf{[S5]}$$

yielding:

$$XC_2(\mathbf{r}_1,\ \mathbf{r}_2,\ \tau) = U^2\left(\frac{\mathbf{r}_1-\mathbf{r}_2}{2}\right)\cdot\sum_k U^2\left(\frac{\mathbf{r}_1+\mathbf{r}_2}{2}-\mathbf{r}_k\right)\cdot\langle\delta f_k(t+\tau)\cdot\delta f_k(t)\rangle_t. \quad \textbf{[S6]}$$

As can be seen, the cross-correlation term is multiplied by a weighting function

$$U^2\left(\frac{\mathbf{r}_1-\mathbf{r}_2}{2}\right),$$

which depends on the distance between pixels $\mathbf{r}_1$ and $\mathbf{r}_2$. As can be seen the resulting image corresponds to the pixel in the geometric middle of $\mathbf{r}_1$ and $\mathbf{r}_2$:

$$I_2(\mathbf{r}') = I_2\left(\frac{\mathbf{r}_1+\mathbf{r}_2}{2}\right) = XC_2(\mathbf{r}_1,\ \mathbf{r}_2,\ \tau). \quad \textbf{[S7]}$$

For instance the second-order SOFI image value for pixel $\mathbf{r}_i$ can be obtained by using its neighboring pixels $\mathbf{r}_{i-1}$ and $\mathbf{r}_{i+1}$ by calculating the cross-cumulant XC_2 ($\mathbf{r}_{i-1}$, $\mathbf{r}_{i+1}$,τ). In a 2D image for each pixel there are four such directly neighboring pixels. Also pixels further away, such as $\mathbf{r}_{i-k}$ and $\mathbf{r}_{i+k}$ can in principle be chosen to apply the cross-cumulant approach. Because of the weighting function, however, significant contributions to the signal are only expected for pixels that are within the FWHM of the nth power of the PSF. Even though no additional resolution is gained, the additional information can be used to reduce the noise in SOFI images, by adding up cross-cumulants, which correspond to the same SOFI image pixel. This is especially useful when short acquisition times are used. This allows analysis of datasets containing as few as 100 frames, which is shown in *Simulation Results*. The cross-cumulant approach cannot only be used to reduce the noise in a SOFI image but also to achieve shot noise-free images as described in the next paragraph. Interestingly using the cross-cumulant approach, one can calculate SOFI image pixels, which lie in between real pixels. This is achieved by correlating directly neighboring pixels $\mathbf{r}_i$ and $\mathbf{r}_{i+1}$.

Taking together the cross-cumulant and the time lag-integrated approach, the information present in the dataset is used in the most efficient way. However, from the perspective of computational time, this might not be necessary for all datasets. Already the very simple approach just using the zero time lag cumulants for a pixel lead to satisfying results.

Shot Noise-Free SOFI Images. As a consequence from the cumulants approach shot-noise-free SOFI images can be achieved in two ways.

1. By omitting time lags of $\tau = 0$ using the time lag-integrated SOFI approach. The zero time lag is equivalent to the multiplication of the fluctuations with themselves without time shifting. Therefore, shot noise will not be cancelled out. Any other time lag will lead to the annihilation of shot noise, because it is not correlated in time.
2. By using the cross-cumulant approach only and omitting the auto-cumulant (cumulants obtained from the same pixel time series). Using this approach, time lags of zero can be used and still images without shot noise will be achieved, because shot-noise from different pixels is not correlated at any time lag.

Simulation Results. We simulated fluorescence signals stemming from two emitters separated by a distance of $1.2\cdot\omega_0$, where ω_0 is the width of a 1D Gaussian PSF. The signal was sampled on a $\omega_0/20$ pixel grid. Both emitters exhibit the same constant blinking rate of 10% (Figs. S1 and S2) resp. 50% (Fig. S3) of the frame-rate. The simulations include shot noise based on the signal strength (which for the first simulation is 50,000 photons per time unit for the area under the Gaussian PSF for each emitter; for the second simulation 50,000 resp. 33,000 photons and the third simulation 5,000 photons, which corresponds to a maximum of 100 photons in the center of each emitte'rs PSF, on top of 20 background photons per pixel) and were done for 20,000 (Figs. S1 and S2) resp. 100 (Fig. S3) frames. In addition to that we added a 20% background (compared with the signal strength) in the simulation in Fig. S3.

In the first simulation we compared the resolving power of SOFI using the two different cumulants formulas (Eqs. **S1** and **S2**) for different time lag settings. Fig. S1 shows when the use of the approximated cumulants formula (Eq. **S2**) is justified. In the limiting case of time lags of $\tau_i = 0$ both cumulants formulas are identical and thus yield the same result (Fig. S1 *a* and *b*). However, for different time-lag settings only the exact cumulant formula will lead to a substantially increased resolution (Fig. S1 *c* and *d*).

In a second simulation we show the brightness scaling of SOFI for emitters that have different molecular brightnesses. For this reason, we set the molecular brightness ratio to 1:0.66 for the two emitters. The result can be seen in Fig. S2. The initial brightness

difference will increase when proceeding to higher-order cumulants. The higher the order calculated the bigger the difference in the SOFI signal. This leads to the masking effect.

In our third simulation, we compared the cross-cumulant approach to SOFI with the conventional cumulant approach, where the cumulants are computed only for the fluctuations from the same pixel. In the cross-cumulant approach, we compute the signal for the SOFI image by calculating the cumulants for pixels within a certain neighborhood of the pixel of interest. This way the SOFI value for a specific pixel can be calculated multiple times, each time using different neighboring pixels. Subsequent summation over all cross-cumulants for this specific pixel leads to a noise reduction. In Fig. S3 we computed the SOFI image out of only 100 frames, showing that this approach can efficiently reduce the acquisition time. Compared with common spatial averaging methods in image processing applications, the cross-cumulant approach specifically improves the signal-to-noise ratio of the SOFI image. This means no smoothing/blurring is applied to reduce the noise.

1. Mendel JM (1991) Tutorial on higher-order statistics (spectra) in signal-processing and system-theory: Theoretical results and some applications. *Proc IEEE* 79:278–305.

2. Smith PJ (1995) A recursive formulation of the old problem of obtaining moments from cumulants and vice versa. *Am Stat* 49:217–218.

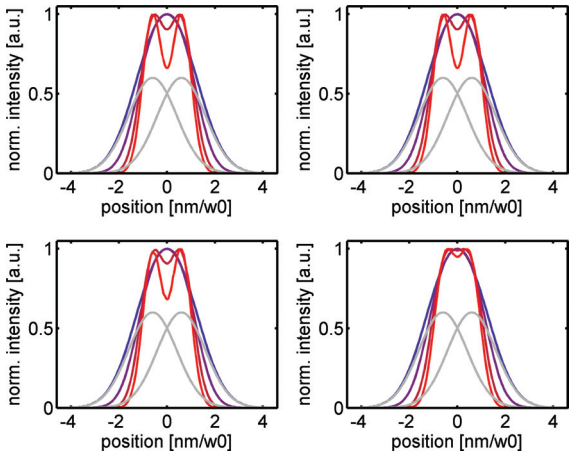

Fig. S1. Simulated SOFI 1D intensity cross-sections. Simulated are two close-by emitters fluctuating at a constant blinking rate of 10% of the frame rate and having identical molecular brightnesses (50,000) to demonstrate the resolving ability of SOFI using different time lags for the calculation of exact versus approximated cumulants. The dotted lines represent the individual diffraction limited PSFs of the two emitters. From blue to red: increasing cumulants orders [orders: 1 (original), 2, 4, 6]. (*a*) All time lags are zero ($\tau_i = 0$), using the exact formula (Eq. **S1**) for the cumulants. (*b*) Same as *a* but using the approximated formula for the cumulants (Eq. **S2**) yielding the same result as *a*. (*c*) Cumulants calculated for time lags ($\tau_i = \tau + 1$, where i is measured in units of frames) using the exact formula. (*d*) Same as *c* but using the approximated formula from cumulants. As can be seen, in this case the resolving ability from the approximated cumulants is compromised.

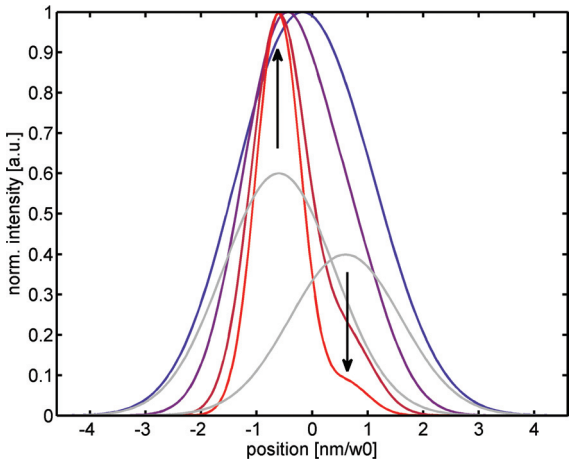

Fig. S2. Simulated SOFI 1D intensity cross-sections. Simulated are two close-by emitters fluctuating at a constant blinking rate of 10% of the frame rate having different molecular brightness (50,000:33,000) to demonstrate the intensity scaling of SOFI images for different cumulant orders. The gray lines represent the individual diffraction limited PSFs of two close-by emitters. From blue to red: increasing cumulants orders [orders: 1 (mean intensity), 2, 4, 6]. Clearly, the two emitters cannot be resolved in the original image. At higher cumulants orders, the PSF is shrinking, but at the same time, the signal stemming from the dim emitter gets buried in the tail of the bright PSF so that they can not be resolved even at higher orders. Note that the intensities are scaled to the maximum value.

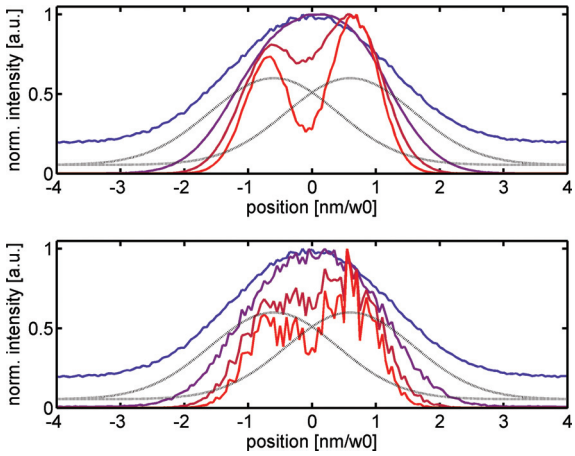

Fig. S3. Simulated SOFI 1D intensity cross-sections. We simulated two close-by emitters fluctuating at a constant blinking rate of 50% of the frame-rate and having identical molecular brightnesses (100 in the center of each emitter PSF) on top of a 20% (compared with the brightness of the center of the emitters PSF) random background was added. This simulation shows the effect of the cross-cumulant approach on the noise in a SOFI image. (*Lower*) The conventional SOFI approach is shown; solely calculating the zero time lag cumulants for each pixel. (*Upper*) The summation over cross-cumulants achieved by correlating pixels within a neighborhood of ± 9 pixels from the pixel of interest is shown. From blue to red: increasing cumulants orders [orders: 1 (mean intensity), 2, 4, 6]. Note that the mean intensity profile is offset because of uncorrelated background.

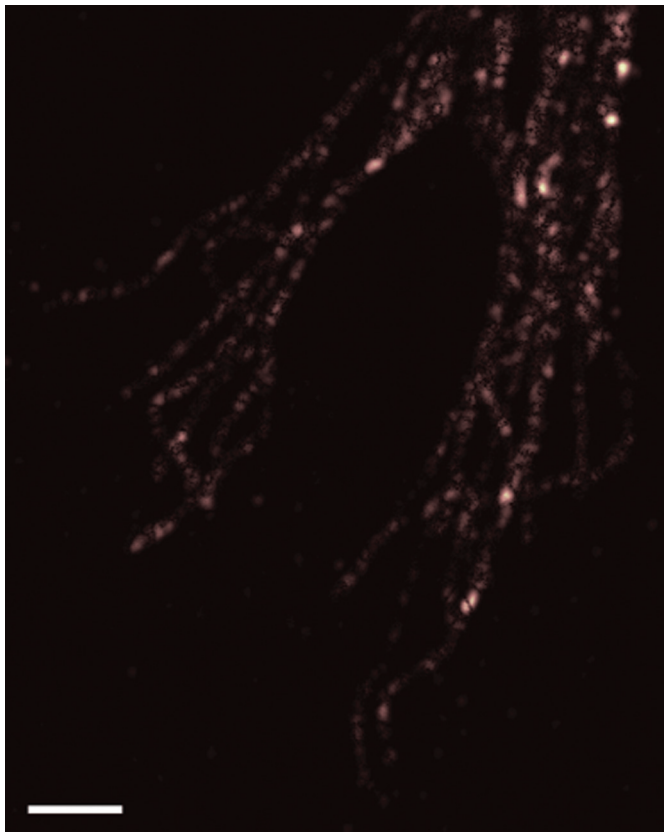

Fig. S4. Fourth-order SOFI image of fibroblasts. Shown is the fourth-order SOFI image as obtained from the fibroblast sample. As can be seen, the intensity range of the SOFI image is so large that a satisfying image cannot be displayed. (Scale bar: 2 μm.)